Generalized in-line digital holographic technique based on intensity measurements at two different planes

Guohai Situ, James P. Ryle, Unnikrishnan Gopinathan, and John T. Sheridan*

School of Electrical, Electronic and Mechanical Engineering, University College Dublin, Belfield, Dublin 4, Dublin, Ireland

*Corresponding author: john.sheridan@ucd.ie

Received 8 June 2007; revised 15 October 2007; accepted 14 December 2007;
posted 20 December 2007 (Doc. ID 83951); published 8 February 2008

In-line digital holography based on two-intensity measurements [Zhang *et al.* Opt. Lett. **29,** 1787 (2004)], is modified by introducing a π shifting in the reference phase. Such an improvement avoids the assumption that the object beam must be much weaker than the reference beam in strength and results in a simplified experimental implementation. Computer simulations and optical experiments are carried out to validate the method, which we refer to as position-phase-shifting digital holography.

OCIS codes: 090.1760, 100.3010.

1. Introduction

In digital holography (DH), the hologram is digitized and the object wavefront is numerically reconstructed by a computer. This technique has received increasing attention since a CCD camera was first used to acquire holographic data in 1994 [1]. DH can easily reconstruct the object wave at different planes by digital refocusing and direct evaluation of the phase distribution of the object wave. Recent advances in fast-speed, high-resolution optoelectronic imaging devices [e.g., CCD and complementary metal-oxide semiconductor (CMOS)] have opened up tremendous potential for the use of DH in many fields such as deformation analysis and shape measurement [2,3], particle tracking [4], microscopy [5,6], encryption [7], object recognition [8,9], and data compression [10].

Initially, digital holograms were recorded using an off-axis geometry. However, due to the angle between the reference and object beams, off-axis DH does not use the available space-bandwidth product (SBP) of the CCD. To eliminate these limitations, in-line DH was developed [11–15] with methods of off-axis [11] phase retrieval [12,13] or phase shifting [14,15] being used for reconstruction. In the latter case, at least three stepwise phase retardation is introduced in the reference beam to remove the overlapped zero-order and conjugate images [16]. A defocused twin image may be present when calibration error exists in phase shifting [17], and this diffractive pattern degrades the quality of the reconstructed image. Error compensation algorithms such as averaging technique [15], iteration postprocess [18,19], and frequency shifting [20] have been applied to eliminate or minimize such noise. Recently, in [21] an algorithm for reconstructing the wavefront was proposed and numerically verified. Rather than using phase-shifting holograms, this method uses two holograms, recorded at two different planes separated by a small distance perpendicular to the propagation direction, for reconstruction. In this method, the simple approximation $\exp[ju] \approx 1 + ju$ is valid when $u \ll 1$ is utilized to remove the zero-order image, and then an algebraic manipulation in the Fourier domain is used to eliminate the twin image. This idea can actually be traced back to 1951, when Bragg and Rogers [22,23] proposed the two-holograms-substraction method in an attempt to remove the twin image. The basic principle has recently found applications in x-ray holography [24,25]. However, as stated, this approximation requires that the object wave should be weak in comparison to the reference, making it sensitive to noise.

In a recent paper [26], we proposed an algorithm to eliminate the weak object approximation by use of a

0003-6935/08/050711-14$15.00/0

two-step phase shifting in the reference beam. In this paper, we present the theoretical analysis and carry out optical experiments as well as numerical simulations to demonstrate this method. Since the improvement involves shifts both in phase and in axial positions, we refer to it as position-phase-shifting digital holography (PPSDH), (used later). In Section 2, we first describe the basic principle of the algorithm. In Section 3, computer simulations are carried out to verify this method, and then in Section 4 experimental results are presented for demonstration. Conclusions are drawn in Section 5.

2. Basic Principle

The basic principle is illustrated using the schematic shown in Fig. 1. A laser beam is split into a reference beam and a beam to illuminate the object using a beam splitter (BS). The reference is reflected by a mirror and is combined with the object beam reflected from the object. The resulting interference pattern is recorded in two planes located at distances z and $z + \Delta z$ from the object plane. These two patterns can be written in the form of

$$I_{11}(x_1, y_1) = |r + u_1(x_1, y_1)|^2, \tag{1}$$

$$I_{21}(x_2, y_2) = |r + u_2(x_2, y_2)|^2, \tag{2}$$

where r stands for the reference plane wave and $u_1(x_1, y_1)$ and $u_2(x_2, y_2)$ are the diffraction patterns of the object $u_0(x_0, y_0)$ at the recording planes z and $z + \Delta z$ from the object. These two fields can be, respectively, expressed using the Rayleigh–Sommerfeld formula [27] as

$$\begin{aligned} u_i(x_i, y_i) &= \mathcal{P}\{u_0(x_0, y_0); z_i\}, \\ &= -\frac{1}{2\pi}\int\int u_0(x_0, y_0)\frac{\partial}{\partial z_i}\left[\frac{\exp[jkr_i]}{r_i}\right]\mathrm{d}x_0\mathrm{d}y_0, \end{aligned} \tag{3}$$

where $i = 1, 2$, $z_1 = z$, $z_2 = z + \Delta z$, $r_i = [(x_i - x_0)^2 + (y_i - y_0)^2 + \mathcal{Z}_i^2]^{1/2}$, $k = 2\pi/\lambda$ is the wavenumber of the light, and the operator $\mathcal{P}\{\cdot; \Delta z\}$ stands for the propagation in free space over a distance Δz. Introducing a phase retardation π in the reference beam, we obtain an additional two patterns at the two recording planes:

$$I_{12}(x_1, y_1) = |-r + u_1(x_1, y_1)|^2, \tag{4}$$

$$I_{22}(x_2, y_2) = |-r + u_2(x_2, y_2)|^2. \tag{5}$$

Manipulating Eqs. [(1)–(4)] and [(2)–(5)] and discarding some constant factors, result in two patterns:

$$\Delta I_1(x_1, y_1) = u_1(x_1, y_1) + u_1^*(x_1, y_1), \tag{6}$$

$$\Delta I_2(x_2, y_2) = u_2(x_2, y_2) + u_2^*(x_2, y_2). \tag{7}$$

We can see from these equations that the zero-order image has been removed. From Eqs. (6) and (7), we note that there is a clear relation between $u_1^*(x_1, y_1)$ and $u_2^*(x_2, y_2)$:

$$u_1^*(x_1, y_1) = \mathcal{P}\{u_2^*(x_2, y_2); \Delta z\}. \tag{8}$$

This relation can be used to cancel out the twin image. To do so, apply the propagation operator to $\Delta I_2(x_2, y_2)$, and then subtract the resulting complex amplitude from $\Delta I_1(x_1, y_1)$. That is,

$$\begin{aligned} \delta I(x_1, y_1) &= \Delta I_1(x_1, y_1) - \mathcal{P}\{\Delta I_2(x_2, y_2); \Delta z\} \\ &= u_1(x_1, y_1) + u_1^*(x_1, y_1) \\ &\quad - \mathcal{P}\{u_2(x_2, y_2); \Delta z\} - \mathcal{P}\{u_2^*(x_2, y_2); \Delta z\} \\ &= u_1(x_1, y_1) - \mathcal{P}\{u_2(x_2, y_2); \Delta z\} \\ &= u_1(x_1, y_1) - \mathcal{P}\{u_1(x_1, y_1); 2\Delta z\}. \end{aligned} \tag{9}$$

The last part of Eq. (9) holds because of the linearity of propagation: $u_2(x_2, y_2) = \mathcal{P}\{u_1(x_1, y_1); \Delta z\}$ [27]. It is easy to extract $u_1(x_1, y_1)$ from the above equation in the Fourier domain,

$$\delta\mathcal{I}(\xi, \eta) = \mathcal{U}_1(\xi, \eta)[1 - \mathcal{H}(\xi, \eta; 2\Delta z)], \tag{10}$$

where $\mathcal{H}(\xi, \eta; 2\Delta z)$ is the free space transfer function over a distance $2\Delta z$; and $\mathcal{U}_1(\xi, \eta)$ is the Fourier transform of $u_1(x_1, y_1)$. This equation indicates that $\delta\mathcal{I}(\xi, \eta)$, calculated directly from the recorded holograms, can be specified by the Fourier transform of the object and a transfer function $\mathcal{H}(\xi, \eta; 2\Delta z)$, which can be numerically constructed. Therefore it is straightforward to calculate the object wavefront at the first recording plane,

$$u_1(x_1, y_1) = \mathcal{F}^{-1}\left\{\frac{\delta\mathcal{I}(\xi, \eta)}{1 - \mathcal{H}(\xi, \eta; 2\Delta z)}\right\}, \tag{11}$$

where $\mathcal{F}^{-1}\{\cdot\}$ stands for the inverse Fourier transform. Then taking the inverse Fresnel transform over a distance $-z$ of the resulting complex amplitude results in object function $u_0(x_0, y_0)$.

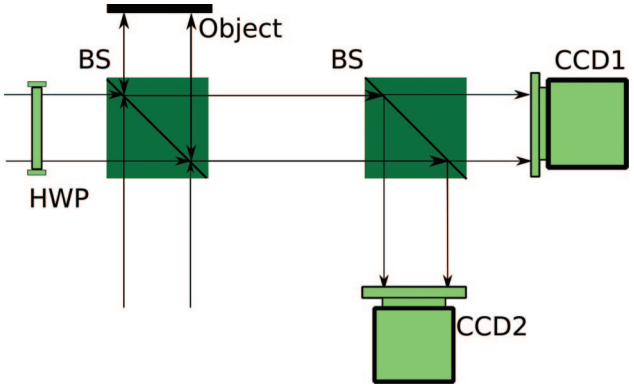

Fig. 1. (Color online) Setup of the in-line DH recording system. HWP, half-wave plate; BS, beam splitter.

3. Computer Simulation

In this section, we perform computer simulations to test the proposed method. As described in Section 2, the reconstruction involves a numerical construction transfer function $\mathcal{H}(\xi, \eta; 2\Delta z)$, and a diffraction over a distance z. Usually, Δz is so small that the Fresnel approximation is not valid. The Rayleigh–Sommerfeld formula should be used to evaluate the transfer function $\mathcal{H}(\xi, \eta; 2\Delta z)$. This can be easily done by examining Eq. (3), from which we can write the impulse response in the form of

$$h(x_0, y_0; x_i, y_i; z_i) = \frac{1}{2\pi} \frac{\partial}{\partial z_i}\left[\frac{\exp[jkr_i]}{r_i}\right]. \quad (12)$$

The corresponding transfer function is the Fourier transform of Eq. (12):

$$\begin{aligned}\mathcal{H}(\xi, \eta; z_i) &= \mathcal{F}\{h(x_0, y_0; x_i, y_i; z_i)\} \\ &= \exp\{-jkz_i[1 - (\lambda\xi)^2 - (\lambda\eta)^2]^{1/2}\}. \end{aligned} \quad (13)$$

Replacing z_i with $2\Delta z$, we obtain $\mathcal{H}(\xi, \eta; 2\Delta z)$. Numerically, this transfer function can be discretely evaluated as follows according to the sampling theory,

$$\mathcal{H}(m, n; z_i) = \exp\left\{-jkz_i\left[1 - \left(\frac{\lambda m}{M\delta x}\right)^2 - \left(\frac{\lambda n}{N\delta y}\right)^2\right]^{1/2}\right\}, \quad (14)$$

for $m = 0, 1, \ldots, M - 1$ and $n = 0, 1, \ldots, N - 1$, and where δx, δy are the sampling intervals in the spatial domain, and M and N are the number of samples in x and y directions, respectively. In our case, δx and δy are the pixel sizes of the CCD camera, and $\delta x = \delta y = 7.6$ μm. The effect of Rayleigh–Sommerfeld diffraction can then be evaluated by the method of angular spectrum propagation [28–32].

To test the proposed technique, we employ the optical system schematically shown in Fig. 2 for simulations. A three-dimensional (3D) transmission object is simulated using an image volume, which in this case consists of three real images with an adjacent separation of $d = 20$ mm as in Fig. 2. Each of these image (512×512 pixels in size) is of transparent background and contains one black letter (U, C, and D, respectively) of 100×84 pixels in size at different locations, making it convenient for illustration. The transparent background means that the transmittance in this area is unity, while the black letters have a transmittance of zero. The distance from the CCD to the nearest image plane is $z = 100$ mm. We assume the illumination wavelength $\lambda = 0.6328$ μm, and the pixel pitch of the CCD is $\delta x = \delta y = 7.6$ μm. The object wavefronts at two recording planes $u_1(x_1, y_1)$ and $u_2(x_2, y_2)$ were calculated by assuming that the input plane wave is sequen-

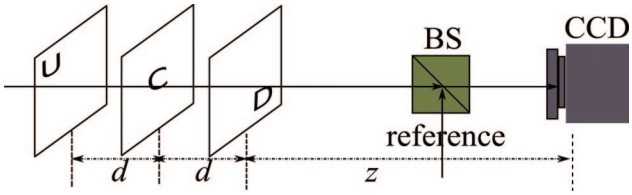

Fig. 2. (Color online) Schematic for computer simulations. BS, beam splitter; reference, reference beam. The object volume is used to simulate a 3D object.

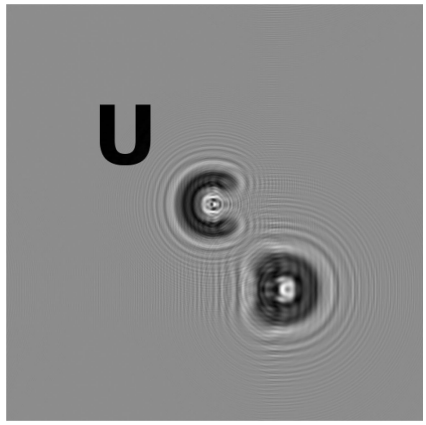

(a)

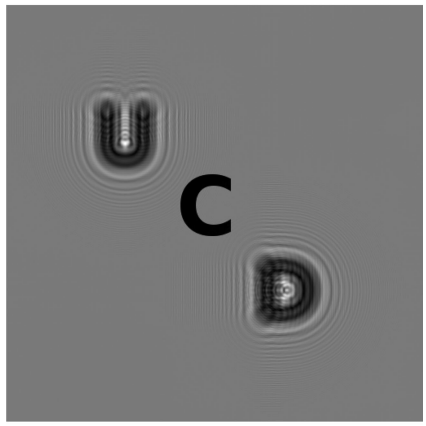

(b)

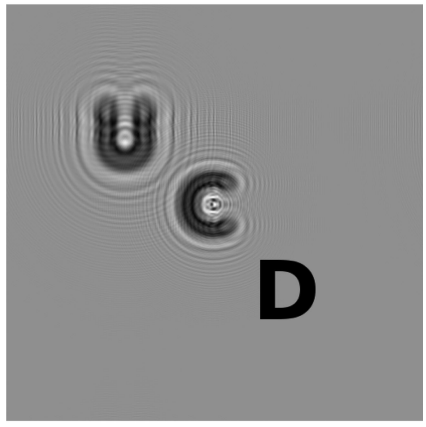

(c)

Fig. 3. Simulation results of the reconstruction of the three letters at the best focus distance of (a) U, 140 mm; (b) C, 120 mm; (c) D, 100 mm from the CCD plane.

tially modulated in amplitude by the three images, and then propagated over a distance z and $z + \Delta z$, where $\Delta z = 0.5$ mm, respectively. In the numerical computation, the object images were embedded into a 1024×1024 black window in order to accurately model the SBP of the object. The resulting complex amplitudes were then interfered with a plane reference wave of unity amplitude in the camera plane, according to Eqs. (1), (2), (4), and (5), to generate four holograms. With these holograms, it is easy to numerically reconstruct the 3D object wavefront using the proposed algorithm. Figures 3(a)–3(c) show the reconstruction of the three letters "U," "C," and "D" at the planes of $z + 2d = 140$, $z + d = 120$, and $z = 100$ mm from the CCD. We can see that only one corresponding letter is best focused at each plane, whereas the other two appear as defocused patterns. This indicates that the 3D object is reconstructed successfully.

4. Experiment and Analysis

We also carried out an experiment to demonstrate the validation of this method. Before going into the details of the experiment, let us take some time to discuss the determination of the suitable shifting distance Δz of the CCD.

Δz should take values to avoid the dominator of the argument on the right-hand side in Eq. (11) becoming 0. This requires that

$$1 - \mathcal{H}(\xi,\ \eta,\ 2\Delta z) \neq 0. \tag{15}$$

In practice, this is numerically evaluated to make sure there are no zeros. Note that $\mathcal{H}(\xi, \eta; 2\Delta z)$ is a pure phase distribution with unity magnitude and takes the form of Eq. (13); substitution of it into Eq. (15), therefore, requires that

$$k2\Delta z\left[1 - \lambda^2\left(\xi^2 + \eta^2\right)\right]^{1/2} \neq 2l\pi, \tag{16}$$

where $l \in \mathbb{N}$ is any integer. After some simple algebra, this indicates that

$$\Delta z \neq \frac{\lambda}{2} \frac{l}{\sqrt{1 - \lambda^2\left(\xi^2 + \eta^2\right)}}. \tag{17}$$

To roughly estimate its value, we rewrite this equation in discrete form:

$$\Delta z \neq \frac{\lambda}{2} \frac{lN\delta}{\sqrt{N^2\delta^2 - \lambda^2\left(m^2 + n^2\right)}}, \tag{18}$$

in which we have chosen to set $M = N$ and $\delta x = \delta y = \delta$ according to the specification of the CCD camera we used. Thus we can run numerical checks before performing the deconvolution Eq. (11) to ensure stability.

The optical setup used is shown in Fig. 4. It is essentially a Mach–Zenhnder interferometer, which is used to define an in-line holographic recording geometry. He–Ne laser light (wavelength $\lambda = 0.6328$ μm) was first collimated and expanded and then passes through a linear polarizer whose polarization direction along the y axis is indicated in the figure. This beam was then divided by a BS into two paths, one of which illuminates the transmission object (a chrome-coated 10 mm × 10 mm × 1.55 mm soda lime glass forming a transparent pattern "optic," flatness: better than 0.0001″, see [33]), and the other, which passing through a half-wave plate, acts as the reference beam. These two beams were then combined with the second BS, and the resulting interferograms were recorded with a CCD camera mounted onto a motorized motion stage, which was driven by Oriel Encoder Mike actuators, controlled using the 18113 Oriel Mike Control System. The CCD we used in the experiment is an IMPERX IPX-IM48, which has 1000 × 1000 square pixels of size 7.6 μm.

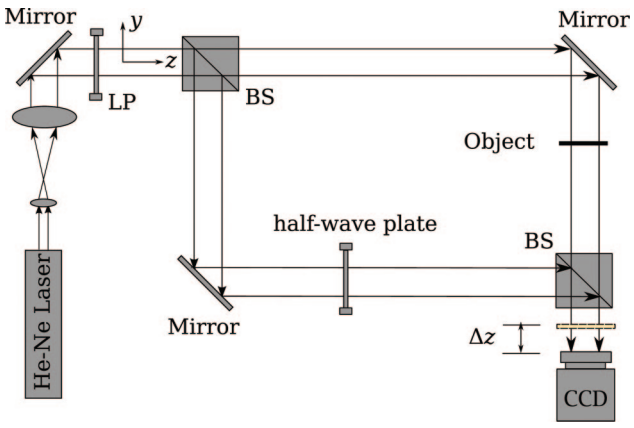

Fig. 4. (Color online) Experimental setup of the proposed technique. BS, beam splitter; LP, linear polarizer.

The four holograms were recorded in the following sequence: first, the phase retardation of the reference was set to be $\phi = 0$, and the hologram $I_{11}(x_1, y_1)$ was recorded at Plane 1, at a distance $z = 267$ mm from the object. Then setting $\phi = \pi$, we recorded the second hologram $I_{12}(x_1, y_1)$. Then we shifted the CCD slightly (choosing $\Delta z = 0.1278$ mm according to the discussion in the previous paragraph. This value in reconstruction may be slightly different with that directly read in the control system because of the dynamic range of the translation stage) along the optical axis to the second recording plane, Plane 2, and recorded the third hologram $I_{22}(x_2, y_2)$, retaining the $\phi = \pi$ phase shift in the reference. Finally, the fourth hologram $I_{21}(x_2, y_2)$ was recorded after setting the phase retardation back to be $\phi = 0$.

The reconstructed image from the four recorded holograms is shown in Fig. 5(a). The corresponding phase component wrapped in $[-\pi, \pi]$ is shown in Fig. 5(b). The dark area in Fig. 5(a) corresponds to the chrome background, through which no light passed during the recording processes. Note that ambiguity appears in the phase map in the chrome-coated area; this is reasonable because there is no definition of phase in the area during the recording processes, and

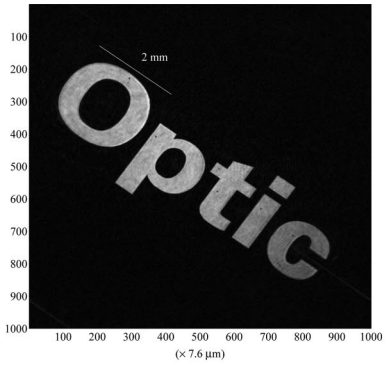

(a)

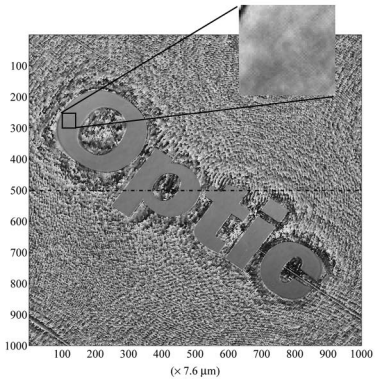

(b)

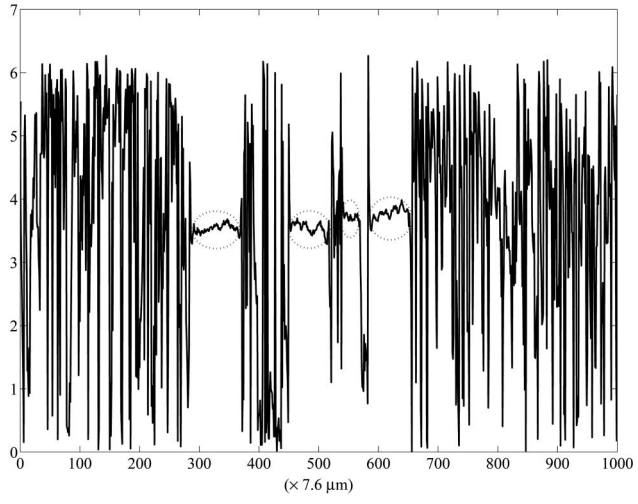

(c)

Fig. 5. Experimental results of the reconstruction image with the proposed technique: (a) magnitude, (b) phase, and (c) the cross section of the phase map as indicated with a dot–dash cross line in (b). Note that those marked with dot ellipses are associating the transparent area.

ambiguity may present in the reconstruction. It is also seen in the phase map that there is fluctuation in the transparent area. This can be seen much more clearer in the cross section of the phase map [marked by a dot–dash line in Fig. 5(b)] as shown in Fig. 5(c), in which the dot ellipses mark those portions. We can make a further step by numerically investigating the

Table 1. Statistic Properties of the Phase Patterns (in Radians)

	O	p	t	i	c
Expectation	3.7456	3.5473	3.5303	3.5168	3.0870
Standard deviation	0.2309	0.1142	0.1697	0.2691	0.2270
Maximum	4.8854	4.3452	4.3246	4.7605	3.8642
Minimum	2.7391	2.8933	2.7478	2.6533	2.0057

statistical property of the phase disturbance in the transparent patterns. The parameters of expectation, the standard deviation, maximum, and minimum values of the phase disturbance of transparent patterns "O," "p," "t," "i," and "c" are shown in Table 1. We can see from the data that the maximum variation of the phase inside the patterns is ~2.88 rad. However, expected variation of larger than 2π with respect to the flatness of the object has not been observed here due to the phase wrapping.

According to Eqs. (6) and (7), the applicability of the reconstruction algorithm assumes that the reference beam be a known constant distribution. This requires the reference wavefront at Planes 1 and 2 should be plane waves, as are usual DH setups. This can be obtained by careful spatial filtering and collimation. If Δz is equal to an integer multiple of λ, the phase at these two planes would theoretically have the same distribution. However, this requirement is difficult to fulfill for practical reasons. Consequently, the two plane reference wavefronts will typically have a constant phase difference. This additional propagation phase can be evaluated, since it is specified by the shifting distance Δz under the paraxial approximation. The deduction of the algorithm in this case is straightforward.

5. Conclusion

We have proposed and demonstrated the use of a phase-shifting technique in combination with the in-line digital holography based on a two-intensity measurement recently proposed in [21]. Use of this technique, which we refer to as PPSDH, eliminates the requirement that the object beam should be much weaker than the reference beam. We have experimentally validated our proposed technique. Although the technique requires four holograms for reconstruction, it needs only two steps of shifting in phase. From the point of view of the number of measurements to be done, there is no advantage of our method over classical phase shifting. Our motivation to pursue this method was not to reduce the number of measurements. Rather it was to address the accuracy of classical phase shifting methods. The accuracy of phase-shifting methods is very sensitive to the phase shifting of the reference beam over a cycle of recording [17–20]. Errors in phase shifts can lead to a situation in which the conjugate term is not fully eliminated; [21] suggested a method to eliminate the need for phase shifting of the reference beam by performing two-intensity measurements in two planes, albeit with the object beam satisfying certain criteria (weak compared to the reference beam). We have

tried to generalize this method and provide an experimental validation. To do so, we have chosen to phase shift the reference beam by 180° and involve four measurements instead of the two suggested in [21]; now the method is less sensitive to phase shifts of the reference beams but is more sensitive to the accuracy of the choice of two planes and how close the reference beam is to a plane beam. In situations when it is not possible to provide accurate phase shifts of a reference beam, (e.g., when a suitable piezoelectric device is not available), our method is a better choice. Furthermore, a compact system, as shown in Fig. 1, can be used to make the recording process faster than in conventional phase-shifting DH, providing an alternative technique for the recording of some fast processes.

The techniques based on intensity measurements at two different planes also opens up a possibility for an in-line digital holograph without using phase shifting. For example, we can capture the object beam intensities, say $|u_1(x_1, y_1)|^2$ and $|u_2(x_2, y_2)|^2$, at Planes 1 and 2. Subtraction of them from the holograms, Eqs. (1) and (2), respectively, also results in Eqs. (6) and (7), although with an additional constant offset in intensity. Phase shifting, or Eqs. (4) and (5), is not necessary in this case.

It is worth noting that if perfect alignment in the DH system is not achieved, a defocused twin image would superpose on the reconstructed image; for example, see Fig. 6. In this case, numerical compensation can be used to improve the reconstruction. Such postprocessing is popular and has become a standard technique in digital interferometry [18–20] and holographic microscopy [34–36]. Currently we are working on the mechanism of the twin image generation and the corresponding compensation technique. In the future we aim to simplify the recording process further (including those discussed in the last paragraph) and apply this technique to microscopy.

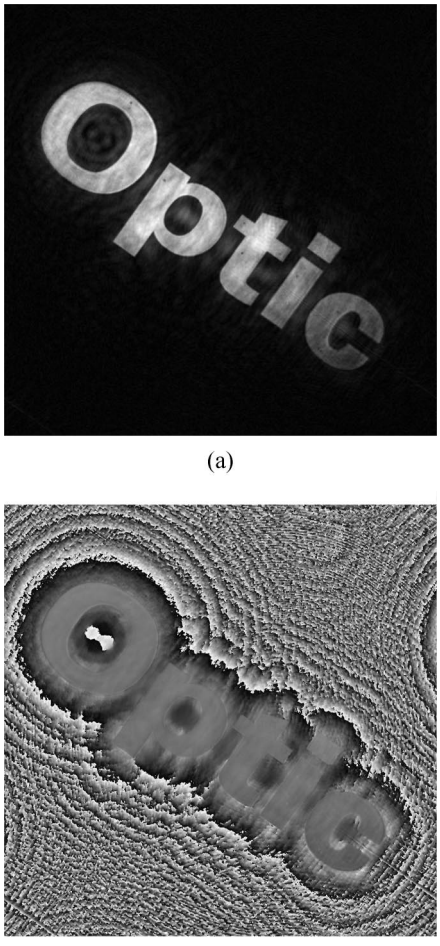

(a)

(b)

Fig. 6. Reconstruction with a twin image superposition: (a) amplitude, (b) phase component.

G. Situ thanks the support of the Irish Research Council for Science, Engineering and Technology (IRCSET). This research is also funded by Science Foundation Ireland and Enterprise Ireland.

References

1. U. Schnars and W. Jüptner, "Direct recording of holograms by a CCD target and numerical reconstruction," Appl. Opt. **33,** 179–181 (1994).
2. S. Seebacher, W. Osten, and W. Jüptner, "Measuring shape and deformation of small objects using digital holography," Proc. SPIE **3479,** 104–115 (1998).
3. G. Pedrini, P. Fröning, H. Tiziani, and F. M. Santoyo, "Shape measurement of microscopic structures using digital holograms," Opt. Commun. **164,** 257–268 (1999).
4. M. Adams, T. Kreis, and W. Jüptner, "Particle size and position measurement with digital holography," Proc. SPIE **3098,** 234–240 (1997).
5. W. Haddad, D. Cullen, J. C. Solem, J. M. Longworth, A. McPherson, K. Boyer, and C. K. Rhodes, "Fourier-transform holographic microscope," Appl. Opt. **31,** 4973–4978 (1992).
6. J. Garcia-Sucerquia, W. Xu, S. K. Jericho, P. Klages, M. H. Jericho, and H. J. Kreuzer, "Digital in-line holographic microscopy," Appl. Opt. **45,** 836–850 (2006).
7. B. Javidi and T. Nomura, "Securing information by use of digital holography," Opt. Lett. **25,** 28–30 (2000).
8. B. Javidi and E. Tajahuerce, "Three-dimensional object recognition by use of digital holography," Opt. Lett. **25,** 610–612 (2000).
9. A. Nelleri, U. Gopinathan, J. Joseph, and K. Singh, "Three dimensional object recognition from digital Fresnel hologram by wavelength matched filtering," Opt. Commun. **259,** 499–506 (2006).
10. E. Darakis, T. J. Naughton, and J. J. Soraghan, "Compression defects in different reconstructions from phase-shifting digital holographic data," Appl. Opt. **46,** 4579–4586 (2007).
11. S. Lai, B. Kemper, and G. von Bally, "Off-axis reconstruction of in-line holograms for twin-image elimination," Opt. Commun. **169,** 37–43 (1999).
12. G. Liu and P. D. Scott, "Phase retrieval and twin-image elimination for in-line Fresnel holograms," J. Opt. Soc. Am. A **4,** 159–165 (1987).
13. Y. Zhang, G. Pedrini, W. Osten, and H. J. Tiziani, "Image reconstruction for in-line holography with the Yang–Gu algorithm," Appl. Opt. **42,** 6452–6457 (2003).
14. I. Yamaguchi and T. Zhang, "Phase-shifting digital holography," Opt. Lett. **22,** 1268–1270 (1997).
15. S. Lai, B. King, and M. A. Neifeld, "Wave front reconstruction by means of phase-shifting digital in-line holography," Opt. Commun. **173,** 155–160 (2000).

16. I. Yamaguchi, J. Kato, S. Ohta, and J. Mizuno, "Image formation in phase-shifting digital holography and applications to microscopy," Appl. Opt. **40,** 6177–6186 (2001).
17. J. Schwider, R. Burow, K.-E. Elssner, J. Grzanna, R. Spolaczyk, and K. Merkel, "Digital wave-front measuring interferometry: some systematic error sources," Appl. Opt. **22,** 3421–3432 (1983).
18. C. S. Guo, L. Zhang, H. T. Wang, J. Liao, and Y. Y. Zhu, "Phase-shifting error and its eliminiation in phase-shiting digital holography," Opt. Lett. **27,** 1687–1689 (2002).
19. X. F. Xu, L. Z. Cai, X. F. Meng, G. Y. Dong, and X. X. Shen, "Fast blind extraction of arbitrary unknown phase shifts by an iterative tangent approach in generalized phase-shifting interferometry," Opt. Lett. **31,** 1966–1968 (2006).
20. M. Atlan, M. Gross, and E. Absil, "Accurate phase-shifting digital interferometry," Opt. Lett. **32,** 1456–1458 (2007).
21. Y. Zhang, G. Pedrini, W. Osten, and H. J. Tiziani, "Reconstruction of in-line digital holograms from two intensity measurements," Opt. Lett. **29,** 1787–1789 (2004).
22. W. L. Bragg and G. L. Rogers, "Elimination of the unwanted image in diffraction microscopy," Nature **167,** 190–191 (1951).
23. G. L. Rogers, "In-line soft-x-ray holography: the unwanted image," Opt. Lett. **19,** 67–67 (1994).
24. T. Q. Xiao, H. J. Xu, Y. J. Zhang, J. W. Chen, and Z. Z. Xu, "Digital image decoding for in-line X-ray holography using two holograms," J. Mod. Opt. **45,** 343–353 (1998).
25. Y. Nishino, T. Ishikawa, K. Hayashi, Y. Takahashi, and E. Matsubara, "Two-energy twin image removal in atomic-resolution x-ray holography," Phys. Rev. B **66,** 092105 (2002).
26. G. Situ and J. T. Sheridan, "A new reconstruction algorithm for in-line digital holography," in *European Conference on Lasers and Electro-Optics, 2007 and the International Quantum Electronics, Conference* (CLEOE-IQEC 2007) (IEEE, 2007), digital OID: 4386033.
27. J. W. Goodman, *Introduction to Fourier Optics,* 3rd ed. (Roberts & Company, 2004).
28. Ê. Lalor, "Conditions for validity of the angular spectrum of plane waves," J. Opt. Soc. Am. **58,** 1235–1237 (1968).
29. D. Mendlovic, Z. Zalevsky, and N. Konforti, "Computation considerations and fast algorithms for calculating the diffraction integral," J. Mod. Opt. **44,** 407–414 (1997).
30. D. Mas, J. Carcia, C. Ferreira, L. M. Bernardo, and F. Marinho, "Fast algorithm for free-space diffraction patterns calculation," Opt. Commun. **164,** 233–245 (1999).
31. B. M. Hennelly and J. T. Sheridan, "Generalizing, optimizing, and inventing numerical algorithms for the fractional Fourier, Fresnel, and linear canonical transforms," J. Opt. Soc. Am. A **22,** 917–927 (2005).
32. B. M. Hennelly and J. T. Sheridan, "Fast numerical algorithm for the linear canonical transform," J. Opt. Soc. Am. A **22,** 928–937 (2005).
33. http://www.edmundoptics.com/onlinecatalog/displayproduct.cfm?productID=1790.
34. A. Stadelmaier and J. H. Massig, "Compensation of lens aberrations in digital holography," Opt. Lett. **25,** 1630–1632 (2000).
35. F. Montfort, F. Charriére, T. Colomb, E. Cuche, P. Marquet, and C. Depeursinge, "Purely numerical compensation for microscope objective phase curvature in digital holographic microscopy: influence of digital phase mask position," J. Opt. Soc. Am. A **23,** 2944–2953 (2006).
36. L. Miccio, D. Alfieri, S. Grilli, P. Ferraro, A. Finizio, L. De Petrocellis, and S. D. Nicola, "Direct full compensation of the aberrations in quantitative phase microscopy of thin objects by a single digital hologram," Appl. Phys. Lett. **90,** 041104 (2007).